第 43 卷 第 10 期 焊 接 学 报 Vol. 43(10):57 − 62, 70
2022 年 10 月 TRANSACTIONS OF THE CHINA WELDING INSTITUTION October 2022

薄板 TC4 钛合金 TIG 电弧和激光焊接接头晶粒尺寸与微观组织

李军兆[1]， 孙清洁[1,2]， 于航[1]， 张鹏程[1]， 刘一搏[2]， 曾宪山[1]
(1. 湖南湘投金天新材料有限公司 益阳 413000; 2. 哈尔滨工业大学 (威海) 威海 264209)

摘要: 对薄板 TC4 钛合金进行 TIG 电弧和激光焊接技术研究, 重点分析了 TIG 焊接电流、焊接速度和激光输出功率对 TC4 钛合金焊接接头晶粒尺寸、微观组织和显微硬度的影响规律. 试验结果表明, 在实现薄板 TC4 钛合金完全熔透的条件下, 激光焊接具有更小热输入, 接头焊缝区和热影响区宽度也显著降低. TIG 焊接接头晶粒尺寸随热输入增加, 呈现增加趋势. 随距焊缝中心位置增加, 焊接接头晶粒尺寸均逐渐降低. TC4 钛合金激光焊接接头焊缝区呈现魏氏组织特征, 针状 α'马氏体细小. 近缝热影响区组织为网篮状 α'马氏体, 而近母材热影响区为未转变 α 相和针状 α'马氏体的双相组织. 随距焊缝中心位置增加, 马氏体生成量逐渐减少, 焊缝显微硬度值呈现降低趋势; 同时相比于 TIG 焊接, TC4 激光焊接接头具有更高的显微硬度.

创新点: (1) 对比分析了薄板 TC4 钛合金 TIG 电弧焊接和激光焊接横截面、微观组织、显微硬度的差异.
(2) 分析了焊接热输入对 TC4 钛合金焊接接头晶粒分布特征的影响规律.

关键词: TC4 钛合金; TIG 焊接; 激光焊接; 微观组织; 晶粒尺寸
中图分类号: TG 442 **文献标识码:** A **doi:** 10. 12073/j. hjxb. 20211015001

0 序言

钛合金因其轻质、高强、耐高温、耐腐蚀等优异性能, 被广泛应用于航空航天、海洋工程、化工及压力容器等领域[1]. 随着我国先进飞行器的发展, 将钛合金应用于管路系统, 相比于传统的不锈钢或铝合金管材, 钛合金管不仅能够承担更大的工作压力, 还能够满足航空航天领域对可靠性及持久性的要求[2-3].

在实际应用过程中, 钛合金管材、板材或型材均会受到空间位置及装配精度局限, 势必要采用合适的焊接方法对其进行连接. 目前, 薄板钛合金常用的焊接方法为钨极氩弧焊接 (TIG), 吴巍等人[4]研究发现钛合金常规 TIG 焊接接头的焊缝和热影响区晶粒严重粗化, 在热影响区粗晶区部位存在硬度的软化区, 随着焊接热输入增加, 硬度值逐渐减小. 吴健文等人[5]采用快频脉冲 TIG 技术搅拌熔池内部液态金属, 进而减小 TC4 钛合金焊缝晶粒和热影响区粗化, 焊缝区组织为网篮状马氏体 α'相.

随着激光焊接的普遍应用, TC4 钛合金激光焊接技术也得到大量研究[6-8]. 南京航空航天大学黄炜等人[9]研究发现 TC4 钛合金激光焊接接头主要分为细晶区、柱状晶区和等轴晶区, 熔合区组织主要为网篮状针状 α'马氏体和未转变的 β 相, 热影响区主要为初生 α 相和针状 α'马氏体. 日本大阪大学 Liu 等人[10]认为随着激光焊接速度的增加, 熔合区的针状 α'马氏体变得更加细小, 使得熔合区硬度值维持在较高的水平. 西安交通大学 Xu 等人[11]研究发现 TC4 激光焊接接头硬度值分布与微观组织密切相关, 焊缝熔合线位置具有最大硬度值, 而随距焊缝中心距离增加, 显微硬度值逐渐减小.

TC4 钛合金焊接接头宏观形貌、微观组织及显微硬度与 TIG 和激光焊接方法及工艺参数密切相关, 因此主要对 TIG 和激光焊接方法下的工艺、组织、性能的相互关系进行系统研究.

1 试验方法

研究所采用的试验材料为 TC4 钛合金, 试样长

收稿日期: 2021 − 10 − 15
基金项目: 湖南省科技创新计划项目 (S2021GXKJCX0287); 湖南省科技创新计划资助 (2022RC1060).

为 100 mm、宽为 100 mm、厚 2.0 mm, 化学成分如表 1 所示. 采用 TIG 和激光表面自熔焊接方法, 焊接方向垂直于板材轧制方向, 焊接示意图如图 1 所示. 施焊前, 采用砂纸对试样表面进行打磨, 并采用 NaOH 和 HCl 溶液对试样进行处理, 以去除表面的氧化膜, 最后用酒精对试样进行冲洗并烘干.

表 1 TC4 钛合金主要化学成分 (质量分数, %)

Table 1 Chemical composition of TC4 alloy

Al	V	Fe	Si	C	N	H	O	Ti
5.5 ~ 6.8	3.5 ~ 4.5	0.30	0.15	0.10	0.05	0.015	0.15	余量

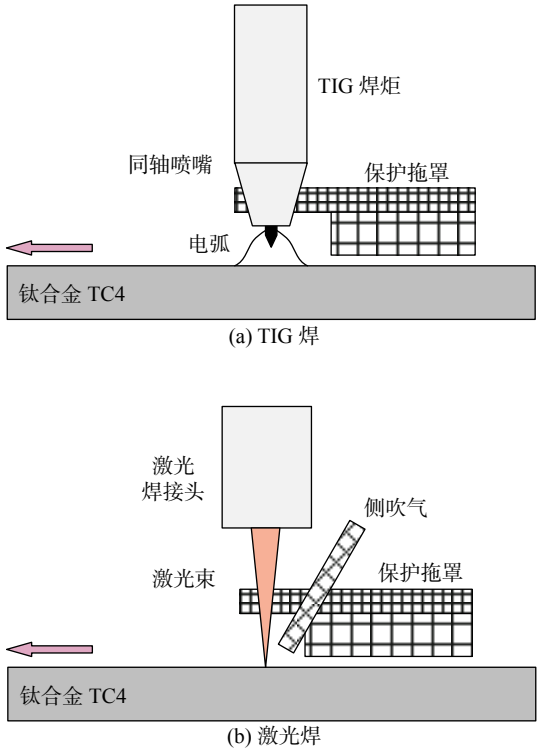

图 1 TC4 钛合金 TIG 和激光焊接示意图

Fig. 1 The TIG and laser welding diagram for TC4 titanium alloy. (a) TIG welding; (b) laser welding

TIG 电弧焊接试验过程中主要研究焊接电流和焊接速度对焊接接头横截面形貌和微观组织的影响规律; 激光焊接主要研究激光输出功率对接头微观组织的影响. TIG 和激光焊接过程中均采用纯氩气对高温焊接熔池区域进行保护, 其中钨极保护喷嘴气体流量为 8 L/min, 焊接拖罩气体流量为 10 L/min.

焊后采用线切割在焊缝相同位置上截取金相试样, 经过磨抛后采用 Kroll 试剂对金相试样进行腐蚀, 采用光学显微镜对焊接接头的组织状态进行分析, 并采用显微硬度计测量接头的显微硬度分布, 焊接接头测量点间距均为 0.2 mm, 加载载荷 1 kg, 持续 15 s.

2 试验结果

2.1 焊接接头宏观形貌及晶粒尺寸

图 2 为不同焊接参数下的 TC4 钛合金 TIG 焊接接头焊缝横截面形貌, 具体数据如表 2 所示. 可以看出 TC4 钛合金 TIG 焊接接头主要分为母材、热影响区和焊缝区. 并且随着焊接电流增加或焊接

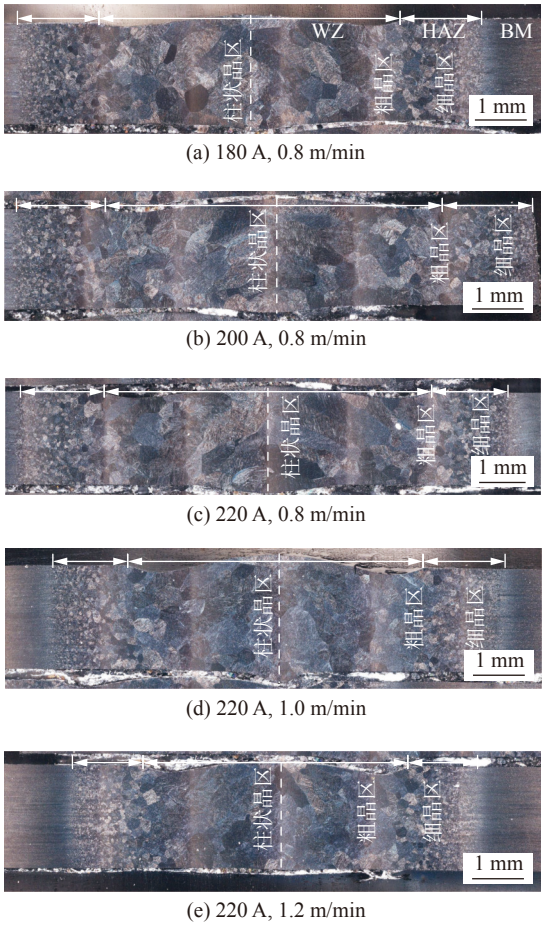

图 2 不同 TIG 焊接参数下的焊缝横截面形貌

Fig. 2 The cross sections of TIG welded joint with various parameters. (a) 180 A, 0.8 m/min; (b) 200 A, 0.8 m/min; (c) 220 A, 0.8 m/min; (d) 220 A, 1.0 m/min; (e) 220 A, 1.2 m/min

表 2　不同 TIG 焊接参数下的焊缝横截面形状参数

Table 2　The shape parameters of TIG weld cross sections with various parameters

序号	焊接电流I/A	焊接电压U/V	焊接速度 v/(m·min^{-1})	热输入Q/(J·mm^{-1})	焊缝宽度d_1/mm	单侧热影响区宽度d_2/mm
1	180	14.3	0.8	116	5.81	1.57
2	200	14.8	0.8	133	6.50	1.71
3	220	15.4	0.8	152	7.04	1.80
4	220	15.2	1.0	120	5.69	1.58
5	220	15.2	1.2	100	5.11	1.36

速度减小, TC4 钛合金焊接接头焊缝区和热影响区宽度逐渐增加, 且焊缝区和热影响区的晶粒尺寸也逐渐增加.

TC4 钛合金焊接接头的组织转变比较复杂, 焊缝区域的晶粒组织形态和尺寸主要取决于最高加热温度、高温停留时间及冷却速率. 钛合金熔点高、导热性能差, 焊接过程中接头在高温停留时间长, 并且焊后冷却过程迅速, 使得焊缝和热影响区的微观组织发生显著变化. 根据晶粒尺寸特征 TC4 钛合金 TIG 焊接接头可以细分为焊缝柱状晶区、焊缝粗晶区、热影响区粗晶区、热影响区细晶区和母材. 其中焊缝柱状晶区晶粒呈 45°夹角从两侧对称向焊缝中心位置生长, 晶粒具有较大的长宽比, 而焊缝粗晶区和热影响区粗晶区晶粒基本呈现等轴状态. 当焊接电流为 220 A、焊接速度为 0.8 m/min 时, 此时具有最大的焊接热输入, 焊缝区表面宽度为 7.04 mm, 单侧热影响区宽度为 1.80 mm, 焊缝中心区域呈现铸态组织特征, 晶粒显著粗化, 为粗大的柱状晶组织.

图 3 为不同参数下的焊缝晶粒尺寸分布特征, 可以发现从焊缝中心向两侧, 晶粒尺寸逐渐减小, 呈现非线性梯度变化特征, 在柱状晶/焊缝粗晶区、焊缝粗晶区/热影响区粗晶区具有最大的晶粒梯度. 随着焊接电流增加或焊接速度降低, 焊缝中心柱状晶区的宽度逐渐减小, 并向粗晶区转变, 焊缝区晶粒尺寸变化趋势逐渐趋于平缓. 特别是当焊接速度增加至 1.2 m/min 时, 焊缝中心区域的晶粒尺寸基本一致, 粗大柱状晶区域减小, 晶粒长宽比降低, 与粗晶区基本具有相似的晶粒尺寸.

图 4 为不同激光焊接参数下的焊缝横截面形貌, 如表 3 所示. 可以看到不同激光焊接功率下的 TC4 钛合金焊缝横截面形貌基本相似, 焊缝区和热影响区宽度变化不明显, 不同激光功率参数下的接头焊缝区宽度为 2.50 mm, 约为 TIG 焊缝区宽度

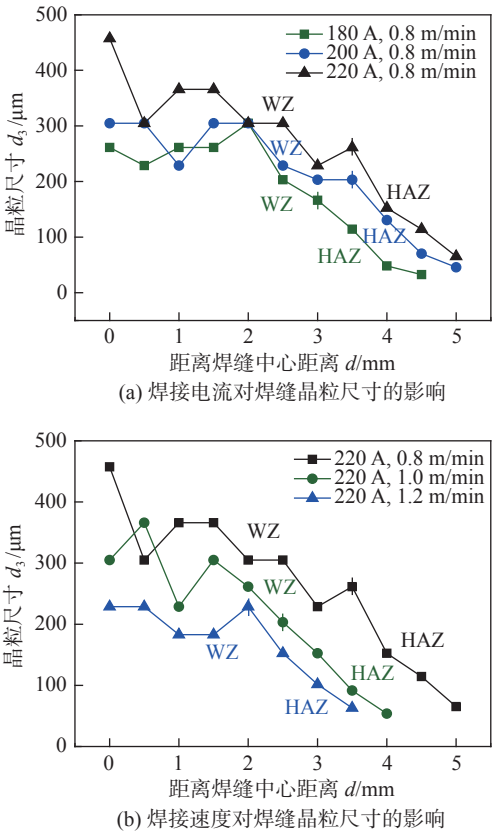

(a) 焊接电流对焊缝晶粒尺寸的影响

(b) 焊接速度对焊缝晶粒尺寸的影响

图 3　不同参数下的焊缝晶粒尺寸分布特征

Fig. 3　The grain distribution characteristics of welded joint with various parameters. (a) effect of welding current on grain size; (b) effect of welding speed on grain size

的 40%; 单侧热影响区宽度为 0.50 mm, 约为 TIG 焊热影响区宽度的 30%. 接头焊缝区主要为柱状晶组织, 具有联生结晶生长的特征, 相比于 TIG 焊接柱状晶尺寸显著降低. 这是由于激光焊接具有较快的加热和冷却速率, 熔池液态金属主要依附于母材半熔化晶粒形核长大, 熔池高温停留时间相对较短, 晶粒来不及长大变凝固. 在热影响区主要分为近缝区的完全转变热影响区, 组织为粗大等轴晶; 以及近母材区的未完全转变热影响区, 组织为的细小等轴晶和板条组织, 主要与最高加热温度有关.

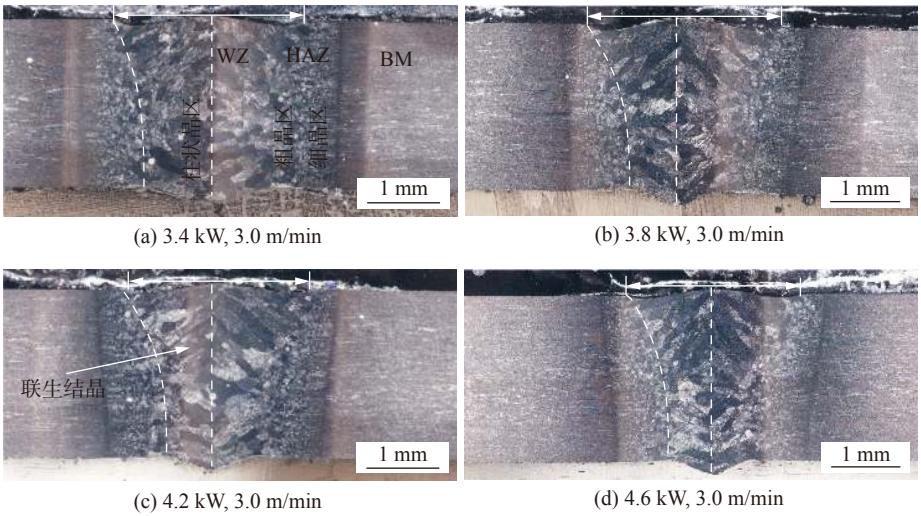

(a) 3.4 kW, 3.0 m/min (b) 3.8 kW, 3.0 m/min

(c) 4.2 kW, 3.0 m/min (d) 4.6 kW, 3.0 m/min

图 4 不同激光焊接参数下的焊缝横截面形貌

Fig. 4 The cross sections of laser welded joint with various parameters. (a) 3.4 kW, 3.0 m/min; (b) 3.8 kW, 3.0 m/min; (c) 4.2 kW, 3.0 m/min; (d) 4.6 kW, 3.0 m/min

表 3 不同激光焊接参数下的焊缝横截面形状参数

Table 3 The shape parameters of laser weld cross sections with various parameters

序号	激光功率P/kW	焊接速度v /(m·min^{-1})	离焦量d_F /mm	热输入Q /(J·mm^{-1})	焊缝宽度d_1 /mm	单侧热影响区宽度d_2 /mm
1	3.4	3.0	0	68	2.61	0.53
2	3.8	3.0	0	76	2.77	0.35
3	4.2	3.0	0	84	2.49	0.38
4	4.6	3.0	0	92	2.50	0.40

2.2 焊缝微观组织与显微硬度

图 5 和图 6 分别为 TIG 焊接 (220 A, 1.2 m/min) 和激光焊接 (4.2 kW, 3.0 m/min) 接头的微观组织特征，虽然两者焊接热源形式有所差异，但是 TC4 钛合金焊接接头不同区域微观组织特征基本相似. 在 TC4 钛合金加热过程中，当温度超过 α/β 转变温度时，TC4 母材中的 α 相向 β 向转变，由于合金元素在 β 相中的扩散系数较大，β 晶粒将快速长大. 在随后的焊缝快速冷却过程中，焊接熔池将会保存原来粗大的 β 晶粒至固相. 因此焊缝组织中为由粗大的 β 柱状晶转变而来的针状马氏体 α'相，高温 β 晶粒的晶界清晰. 此时针状马氏体 α'相具有一定的晶体学相位关系，主要是从 β 晶界向晶内生长. 然而，对比 TIG 焊焊接接头和激光焊接接头组织特征，可以发现，由于激光焊接热输入小、熔池高温停留时间短暂、加热及冷却过程快速，使得 TC4 钛合金焊缝组织的针状 α'马氏体更加细小.

在近缝区热影响区的加热温度超过 α/β 转变温度，α 相全部转变为 β 相，由于此处的加热温度低于焊缝区域，且冷却速度相比于焊缝较快，因此形成 β 等轴晶粒，晶粒尺寸相比于焊缝较小. 在随后的冷却过程中，β 相转变为 α'相. 由于此时熔池的冷却速度相对较大，使得针状马氏体 α'相既能够在 β 晶界形核，又能够在 β 晶内形核，生成网篮组织. 随着距焊缝中心位置的增加，热影响区的加热温度仅能使部分 α 相转变为 β 相，高温为 α + β 双相，由于此时的加热温度较低且冷却速度较快，β 晶粒来不及快速长大，晶粒尺寸较小；与随后的快速冷却使得未转变的 α 保留下来，生成原生 α + 针状马氏体 α'双相组织.

图 7 为 TC4 钛合金 TIG 和激光焊接接头不同区域的显微硬度分布，由图可以发现，激光焊接接头焊缝区显微硬度基本保持在 370 HV，在熔合线位置硬度值达到最高值为 393 HV，在热影响区显微硬度值迅速降低. 激光焊接接头的冷却速度较

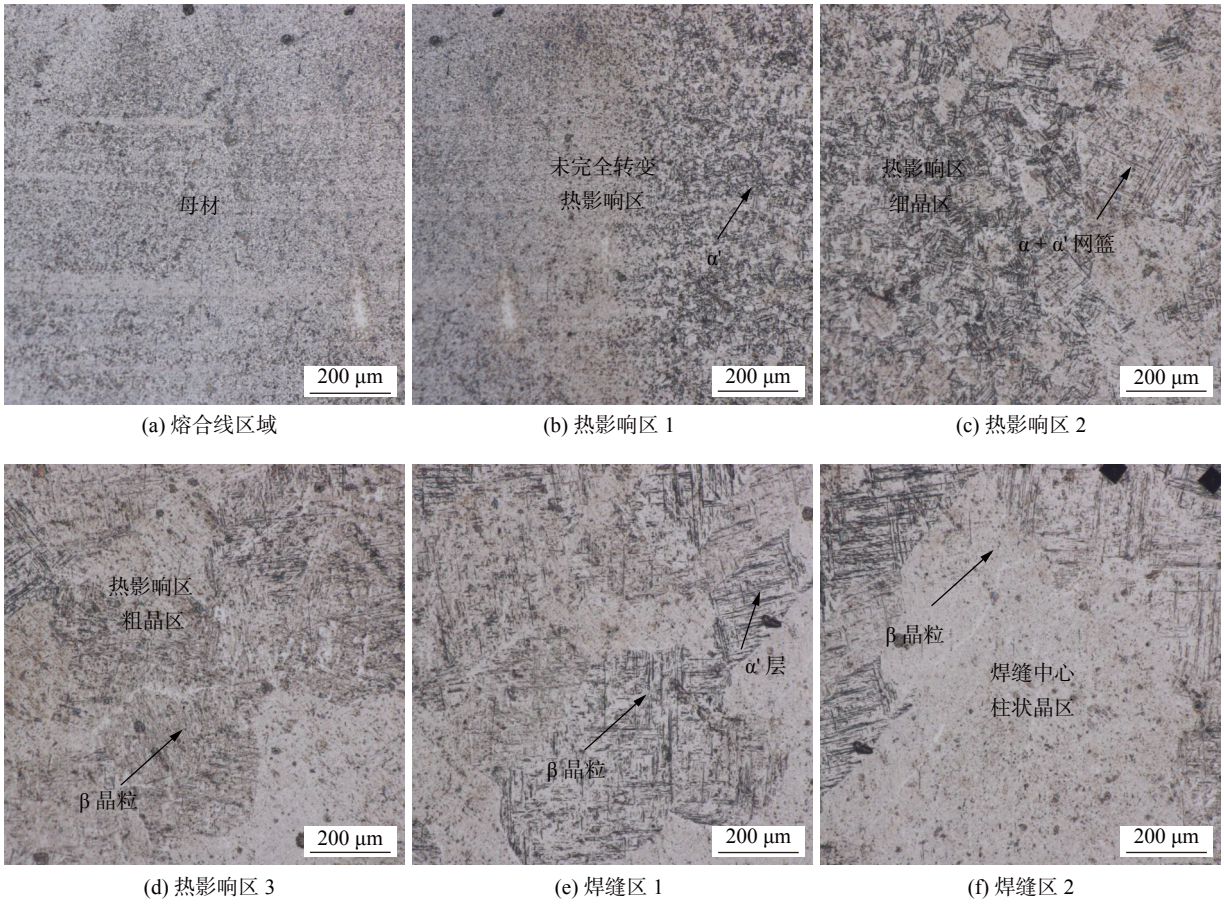

(a) 熔合线区域　(b) 热影响区 1　(c) 热影响区 2

(d) 热影响区 3　(e) 焊缝区 1　(f) 焊缝区 2

图 5　TC4 钛合金 TIG 焊接接头微观组织

Fig. 5　The microstructure of TIG welded joint. (a) fusion line area; (b) heat affected zone 1; (c) heat affected zone 2; (d) heat affected zone 3; (e) weld zone 1; (f) weld zone 2

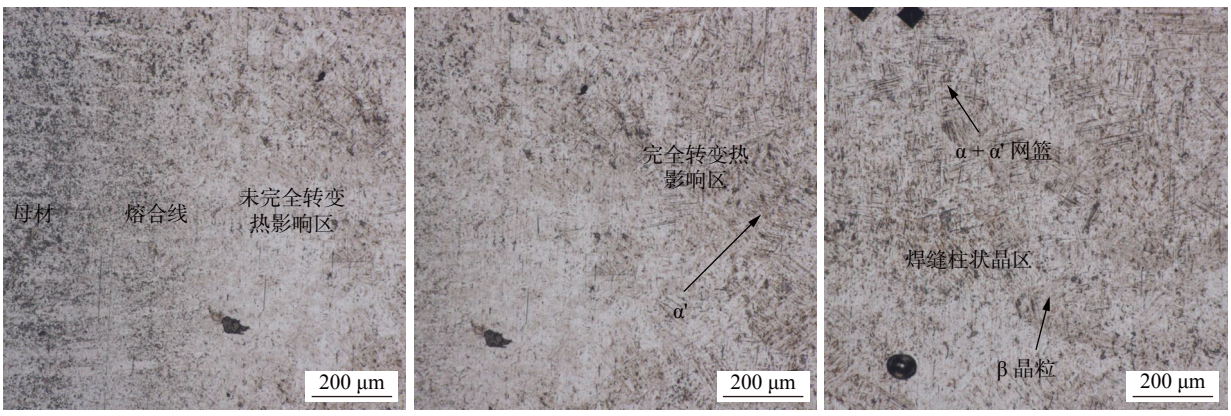

(a) 熔合线区域　(b) 热影响区　(c) 焊缝区

图 6　TC4 钛合金激光焊接接头微观组织

Fig. 6　The microstructure of laser welded joint. (a) fusion line area; (b) heat affected zone; (c) weld zone

快, 导致生成较多的针状 α'相, 使得焊缝显微硬度值相比于母材整体偏高.

此外, TIG 焊接接头的显微硬度值要明显低于激光焊接接头, 焊缝区显微硬度值为 350 HV, 在近缝热影响区粗晶区存在软化区, 显微硬度值达到最低值 300 HV, 随后在热影响细晶区有所增加, 并逐渐降低至母材 320 HV 左右. 这是因为钛合金导热性差, 热影响区近缝区长时间处于过热状态, β 晶粒严重长大, 在随后的冷却过程中, 较快的冷却速度使得未转变的 α 相保留下来, 形成 α + α'双相组织, 在硬度方面体现为熔合线附近粗晶区的显微硬度值降低.

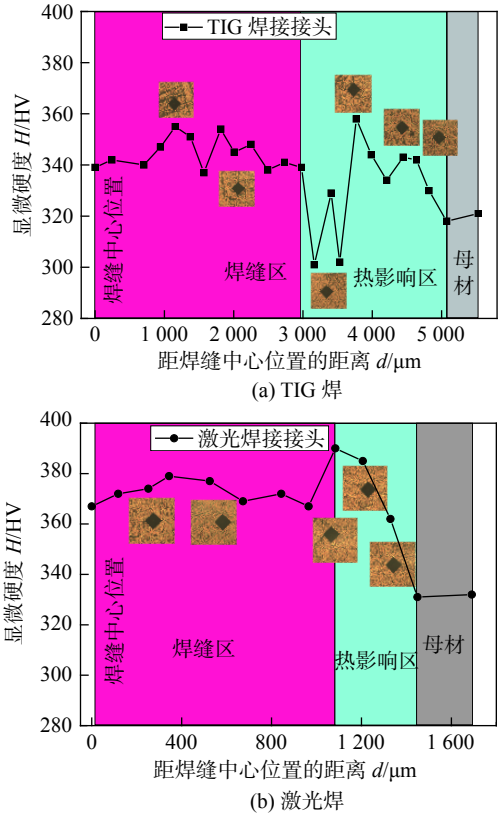

图 7 TC4 合金 TIG 和激光焊接接头显微硬度分布特征

Fig. 7 The microhardness distribution of TIG and laser welded joints. (a) TIG welding; (b) laser welding

3 结论

(1) 在实现 2.0 mm 厚度 TC4 钛合金全熔透条件下, 激光焊接具有较小的热输入和较高的焊接速度, 激光焊接接头焊缝区和热影响区宽度分别为 TIG 焊接接头的 40 % 和 30 %.

(2)TC4 钛合金 TIG 和激光焊接接头晶粒尺寸随距焊缝中心位置的增加逐渐减小. 相比于 TIG 焊接, 激光焊接接头焊缝区柱状晶和热影响区等轴晶的晶粒尺寸均显著减小. 且随着焊接热输入增加, TC4 钛合金 TIG 焊接接头的晶粒尺寸逐渐增大, 而激光焊接接头晶粒尺寸对热输入的敏感性较低.

(3) 相比于 TIG 焊接, TC4 钛合金激光焊接具有快速加热和冷却的特征, 焊缝区呈现魏氏组织特征, 针状 α'马氏体相互交错, 且马氏体更加细小, 接头的显微硬度值相对较高. 而 TC4 钛合金 TIG 焊接接头在近缝热影响区粗晶区存在软化现象, 显微硬度值低于母材.

参考文献

[1] 孙文君, 王善林, 陈玉华, 等. 钛合金先进焊接技术研究现状 [J]. 航空制造技术, 2019, 62(18): 63 − 72.
Sun Wenjun, Wang Shanlin, Chen Yuhua, wt al. Development of advanced welding technologies for titanium alloys[J]. Aeronautical Manufacturing Technology, 2019, 62(18): 63 − 72.

[2] 张颖云, 陈素明, 李波. 激光焊接参数对 1.2mm TC4 钛合金薄板焊缝的影响 [J]. 焊管, 2019, 42(9): 26 − 31.
Zhang Yinyun, Chen Suming, Li Bo. Influence of laser welding parameters on the weld of TC4 titanium alloy with 1.2 mm thickness[J]. Welded Pipe and Tube, 2019, 42(9): 26 − 31.

[3] 马忠贤, 冯军宁, 胡志杰. 钛及钛合金型材研究进展 [J]. 世界有色金属, 2016, 24: 52 − 53.
Ma Zhongxian, Feng Junning, Hu Zhijie. Research and development of titanium and titanium alloys shapes[J]. World Nonferrous Metals, 2016, 24: 52 − 53.

[4] 吴巍, 程广福, 高洪明, 等. TC4 合金 TIG 焊接头组织转变与力学性能分析 [J]. 焊接学报, 2009, 30(7): 81 − 84,117.
Wu Wei, Cheng Guangfu, Gao Hongming, *et al*. Microstructure transformation and mechanical properties of TC4 alloy joints welded by TIG[J]. Transactions of the China Welding Institution, 2009, 30(7): 81 − 84,117.

[5] 吴健文, 徐孟嘉, 范文艳, 等. 钛合金快频脉冲柔性波形调制 TIG 焊接工艺 [J]. 机械工程学报, 2020, 56(6): 102 − 109.
Wu Jianwen, Xu Mengjia, Fan Wenyan, *et al*. Flexible waveform interpulse TIG welding for titanium alloy[J]. Journal of Mechanical Engineering, 2020, 56(6): 102 − 109.

[6] 杨烁, 宋文清, 曲伸, 等. 薄壁 TC4 钛合金激光焊缝成形试验研究 [J]. 焊接, 2019(1): 5 − 11, 65.
Yang Shuo, Song Wenqing, Qu Shen, *et al*. Experimental study on laser weld appearance of thin-walled TC4 titanium alloy[J]. Welding & Joining, 2019(1): 5 − 11, 65.

[7] Baruah M, Bag S. Influence of pulsation in thermo-mechanical analysis on laser micro-welding of Ti6Al4V alloy[J]. Optics and Laser Technology, 2017, 90: 40 − 51.

[8] 段爱琴, 王振苏, 彭欢, 等. 咬边缺陷对 TC4 钛合金激光焊接头静力拉伸形变特征的影响 [J]. 焊接学报, 2019, 40(11): 54 − 60, 163.
Duan Aiqin, Wang Zhensu, Peng Huan, *et al*. Effect of undercut defect on deformation behavior TC4 titanium alloy laser welded butt joint under static tensile loading[J]. Transactions of the China Welding Institution, 2019, 40(11): 54 − 60, 163.

[9] 黄炜, 王少刚, 李立泽, 等. 钛合金激光焊及其接头的显微组织与力学性能 [J]. 材料开发与应用, 2019, 34(2): 20 − 27.
Huang Wei, Wang Shaogang, Li Lize, *et al*. Laser beam welding of titanium alloy and microstructure and mechanical properties of welded joint[J]. Development and Application of Materials, 2019, 34(2): 20 − 27.

[10] Liu H, Nakata K, Yamamoto N, *et al*. Microstructural characteristics and mechanical properties in laser beam welds of Ti6Al4V alloy[J]. Journal of Materials Science, 2012, 47(3): 1460 − 1470.

[下转第 70 页]

[16] 张敏, 仝雄伟, 李洁, 等. 焊前和焊后调质处理下 25Cr2Ni4MoV 钢焊接接头的组织及性能 [J]. 机械工程材料, 2021, 45(1): 34 − 40.
Zhang Min, Tong Xiongwei, Li Jie, *et al*. Microstructure and properties of 25Cr2Ni4MoV steel welded joint under pre-welding and post-welding quenching and tempering treatment[J]. Materials For Mechanical Engineering, 2021, 45(1): 34 − 40.

[17] Huang K T, Chang S H, Hsieh P C. Microstructure, mechanical properties and corrosion behavior of NbC modified AISI 440C stainless steel by vacuum sintering and heat treatments[J]. Journal of Alloys and Compounds, 2017, 712: 760 − 767.

[18] Jalaja K, Manwatkar S K, Anand P, *et al*. Metallurgical analysis of surface distress on balls during the operation of AISI 440C ball bearings for satellite applications[J]. Engineering Failure Analysis, 2021, 124: 105376.

[19] Puli R, Ram G. Microstructures and properties of friction surfaced coatings in AISI 440C martensitic stainless steel[J]. Surface & Coatings Technology, 2012, 207: 310 − 318.

[20] Veerababu R, Prasad K S, Balamuralikrishnan R, *et al*. Austenite stability and M2C carbide decomposition in experimental secondary hardening ultra-high strength steels during high temperature austenitizing treatments[J]. Materials Characterization, 2018, 144: 191 − 204.

[21] Krishna S C, Tharian K T, Chakravarthi K V A, *et al*. Heat treatment and thermo-mechanical treatment to modify carbide banding in AISI 440C steel: a case study[J]. Metallography, Microstructure, and Analysis, 2016, 5(2): 108 − 115.

[22] Kawata H, Hayashi K, Wakabayashi C, *et al*. Martensite transformation start temperature during quench and austempering in Fe-8Ni-0.2 C alloys[J]. Metallurgical and Materials Transactions A, 2021, 52(4): 1395 − 1408.

[23] Lo K H, Cheng F T, Kwok C T, *et al*. Effects of laser treatments on cavitation erosion and corrosion of AISI 440C martensitic stainless steel[J]. Materials Letters, 2004, 58(1-2): 88 − 93.

[24] Capdevila C, Caballero F G, García de Andrés C. Analysis of effect of alloying elements on martensite start temperature of steels[J]. Materials science and technology, 2003, 19(5): 581 − 586.

[25] Syarif J, Yousuf M H, Sajuri Z, *et al*. Effect of partial solution treatment temperature on microstructure and tensile properties of 440C martensitic stainless steel[J]. Metals - Open Access Metallurgy Journal, 2020, 10(5): 1 − 14.

[26] Manwatkar S K, Bahrudheen A, Tiwari S B, *et al*. Failure analysis of AISI 440C steel ball screws used in the actuator system of a satellite launch vehicle[J]. Journal of Failure Analysis and Prevention, 2017, 17(3): 505 − 512.

第一作者: 代一博，硕士；主要从事高能束焊接技术及接头性能分析研究；E-mail: daiyibo2077@163.com.
通信作者: 房卫萍，高级工程师；主要从事高能束焊接技术及接头性能分析研究；E-mail: fwpln@163.com.

（编辑： 张基隆）

[上接第 62 页]

[11] Xu Z Z, Dong Z Q, Yu Z H, *et al*. Relationships between microhardness, microstructure, and grain orientation in laser-welded joints with different welding speeds for Ti6Al4V titanium alloy[J]. Transactions of Nonferrous Metals Society of China, 2020, 30(5): 1277 − 1289.

第一作者: 李军兆，博士；主要从事钛及钛合金焊接技术研究. 发表论文 10 余篇. Email: 031@goldskycn.com.

（编辑： 张基隆）

ing the difference in feature complexity between laser welding defects and other public datasets used to test adversarial generative networks, a new OCM (one class mixup) module is designed and introduced into the stylegan2-ada for a limited number of samples to improve the performance of the adversarial generative network and accelerate its convergence. The results show that the dataset generated by OCM-stylegan2-ada improves the performance of the classification model by 40% over the original dataset and by 20% over the dataset enhanced with mixup and stylegan2-ada. Also the quality of the visually generated images of weld defects is greatly improved.

Highlights: (1) A generative adversarial network for laser welding defects in small sample can generate high-quality image of welding defects and improve the performance of classification model.

(2) In the case of very few data sets to complete the task, greatly reduce the difficulty of defect classification task, effectively solve the problem of data imbalance.

Key words: welding defects; generative adversarial network; small sample; unbalanced dataset

The forming deviation, mechanical properties and compression failure of porous structures fabricated by laser melting were analyzed XU Rongwei[1], ZHANG Zhenjie[1], LIU Qingyuan[1,2], ZHANG Guanghui[1], LONG Yuhong[1](1. Guilin University of Electronic Technology, Guilin , 541004, China; 2. Huazhong University of Science and Technology, Wuhan, 430074, China). pp 49-56

Abstract: Due to the characteristics of light, high strength and adjustable mechanical properties of porous structure, it is widely used in bone medicine, aerospace and other fields. In order to explore the forming error and compression failure performance of porous structure with selective laser melting (SLM), this paper takes two kinds of porous structure with diamond lattice and spherical six-hole opening as examples to study the compressive mechanical behavior of porous structure manufactured by SLM by theoretical prediction and experimental test. ANSYS software was used to simulate the quasi-static compression of the studied porous structure, and the uniaxial compression experiment of the SLM formed porous structure was carried out. Finally, the deformation process and failure mechanism of the SLM formed porous structure were observed and analyzed combined with the simulation and experiment. After comparison, it is found that the size of the numerical design porous structure deviates from that of the final manufactured structure, resulting in a certain difference between the theoretical value of mechanical properties and the experimental value, but the variation law of stress and strain field is consistent. The experimental results show that when the porosity is 50% ~ 80%, the yield strength and elastic modulus of diamond lattice structure are 31.85 ~ 182.13 MPa and 1.45 ~ 2.30 GPa respectively. The yield strength and elastic modulus of six-hole spherical structure are 35.19 ~ 130.64 MPa and 1.59 ~ 2.90 GPa respectively. The mechanical properties of different porous structures vary with the increase of porosity.

Highlights: (1)The manufacturing error of porous structure formed by selective laser melting technology was investigated and the mechanism of theoretical calculation-experimental deviation was analyzed.

(2)The stress-strain field and mechanical properties of porous structures fabricated by selective laser melting were studied by theoretical prediction and experimental test.

(3)The deformation process and failure mechanism of two heterogeneous porous structures were analyzed by combining simulation and experimental observation.

Key words: porous structure; selective laser melting; compression; deformation process; the failure mechanism

Study on grain size and microstructure of TC4 titanium alloy TIG and laser welding joint LI Junzhao[1], SUN Qingjie[1,2], YU Hang[1], ZHANG Pengcheng[1], LIU Yibo[2], ZENG Xianshan[1](1. Hunan Xiangtou Goldsky New Materials Co., Ltd., Yiyang, 413000; 2. Harbin Institute of Technology at Weihai, Weihai, 264209). pp 57-62,70

Abstract: The TC4 sheet was welded by TIG and laser welding technology. The effects of TIG welding current, welding speed and laser output power on the grain size, microstructure and microhardness of TC4 titanium alloy welded joint were analyzed. The experimental results show that laser welding had a lower heat input, and the width of weld zone and heat-affected zone was significantly reduced under the condition of complete penetration of TC4 titanium alloy sheet. The grain

size of TIG welded joint increased with the increase of heat input. The grain size of welded joint decreased gradually with the increase of distance from the center of weld. The laser welded joint showed the characteristics of widmanstatten structure with the finer acicular martensite α' phase. The microstructure of martensite α' near the heat-affected zone was basket shaped, while the microstructure of martensite α' near the base metal was double phase of untransformed α phase and needle shaped martensite α'. With the increase of the distance from the weld centerline, the martensite content decreased gradually, and the weld microhardness decreased. At the same time, compared with TIG welding, TC4 laser welded joint had higher microhardness.

Highlights: (1) The differences of cross section, microstructure and microhardness of TC4 titanium alloy TIG and laser welded joints were compared and analyzed.
(2) The effect of welding heat input on grain size distribution characteristics of TC4 titanium alloy welded joint was analyzed.

Key words: TC4 titanium alloy; TIG welding; laser welding; microstructure; grain size

Effect of pre-weld heat treatment on the microstructure and mechanical properties of electron beam welded 440C stainless steel joint DAI Yibo[1,2], FANG Weiping[2], PENG Hanlin[2], HU Yongjun[1], YI Yaoyong[2], YI Peng[1,2](1. Guangdong University of Technology, Guangzhou 510006, China; 2. China-Ukraine Institute of Welding, Guangdong Academy of Sciences, Guangzhou 510650, China). pp 63-70

Abstract: The effects of pre-weld heat treatment on microstructure and mechanical properties of electron beam welded 440C stainless steel joint were observed and studied, including annealing as well as quenching and tempering. The characteristics of structure change, joint tension and hardness distribution in the two states are analyzed. The results show that the electron beam weld has a good shape without any microcracks. The microstructure located at the weld consists of martensite and retained austenite, showing a non-equilibrium solidification microstructure, carbon and alloying elements exist in the weld structure in solid solution, and the hardness reaches 398 HV. After quenching and tempering heat treatment before welding, the base metal matrix transforms from ferrite into tempered martensite and retained austenite, and at the same time the carbide part is solid-dissolved into the matrix structure, which increases the matrix structure hardness by 60%. Compared with the annealed state before welding, after electron beam welding, the tensile strength of the welded joint is increased by 20%, and the hardness of the welded heat-affected zone is increased by 35%, but the plastic deformation ability of the joint is reduced, and the fracture occurs in the heat-affected zone.

Highlights: (1) The microstructure and mechanical properties of electron beam welded joints of 440C steel under two heat treatment states of pre welding annealing and quenching and tempering were compared and analyzed.
(2) The carbide particles in welded joints under two heat treatment conditions were counted, and the effects of the changes of carbide particles in different areas on the hardness and mechanical properties of welded joints were analyzed.

Key words: 440C stainless steel; EBW; pre-weld heat treatment; microstructures; mechanical properties

Robot simulation of PDC bit remanufacturing based on laser cladding ZU Haiying, LU Xingyu, SONG Yujie, LI Daqi(Northeast Petroleum University, Daqing 163318, China). pp 71-76

Abstract: In order to reduce the maintenance cost and drilling cycle of PDC bit, a robot was proposed to realize the bit remanufacturing based on laser cladding remanufacturing technology. Based on reverse engineering, data acquisition was carried out on PDC bit, and then data processing and 3D reconstruction were carried out on the obtained bit point cloud data to construct the same 3D model as the solid PDC bit. The software Geomagic Boolean operation was used to obtain the defect part of the workpiece. In software NX1899, isometric plane family Γ was used to intersect the repair part of the drill bit to realize the path planning of the curved part. The trajectory of PDC bit repaired by robot end welding gun was simulated. The software PQart was used to simulate the position of the workpiece relative to the robot in the working environment to realize the trajectory optimization of the robot. The position